Structure, transport and magnetic properties of electron-doped perovskites $R_xCa_{1-x}MnO_3$ (R = La, Y and Ce)

2009 J. Phys.: Condens. Matter 21 196004

(http://iopscience.iop.org/0953-8984/21/19/196004)

J. Phys.: Condens. Matter **21** (2009) 196004 (8pp) doi:10.1088/0953-8984/21/19/196004

Structure, transport and magnetic properties of electron-doped perovskites $R_xCa_{1-x}MnO_3$ (R = La, Y and Ce)

Yang Wang[1], Yu Sui[1,2,3], Xianjie Wang[1] and Wenhui Su[1]

[1] Center for Condensed Matter Science and Technology (CCMST), Department of Physics, Harbin Institute of Technology, Harbin 150001, People's Republic of China
[2] International Center for Materials Physics, Academia Sinica, Shenyang 110015, People's Republic of China

E-mail: suiyu@hit.edu.cn

Received 29 October 2008, in final form 22 March 2009
Published 16 April 2009
Online at stacks.iop.org/JPhysCM/21/196004

Abstract

In this study, the transport and magnetic properties of electron-doped perovskites $R_xCa_{1-x}MnO_3$ (R = La, Y and Ce) were investigated. As the R ion content increases, the crystal structure, resistivity, magnetoresistance, magnetization and related characteristic temperature of these systems all vary systematically. The data show that the variations in the electrical transport properties are mainly dependent on carrier concentration, whereas the magnetic properties of these systems are also dependent on crystal structure. When the carrier concentration exceeds a certain level, charge ordering occurs, leading to the localized electronic state and peaks in the magnetization curves. The magnetic transition temperature T_N can be well described by crystal structural parameters, suggesting that crystal structure and magnetic properties are strongly coupled to each other.

(Some figures in this article are in colour only in the electronic version)

1. Introduction

As typical 3d transition-metal oxides, perovskite manganites $RE_xAE_{1-x}MnO_3$ (RE = rare earth, AE = alkaline earth) have been studied widely in recent years because of their rich physical properties such as colossal magnetoresistance (CMR), phase separation, charge ordering (CO), orbital ordering (OO) and spin glass (SG) behavior [1–6]. Hole-type Mn^{3+}-rich CMR manganese oxides have attracted much attention due to their potential applications in magnetic memory [7–11]. In contrast to the hole-doped phases, electron-doped manganites (namely Mn^{4+}-rich) have not been investigated extensively. Unlike hole-doped manganites, the CMR effect in electron-doped manganites is observed only in a narrow region of the phase diagram [2, 3, 5]. Furthermore, the electron-doped manganites do not exhibit a ferromagnetic (FM) ground state at any composition [12], but FM clusters are considered to exist in the entire antiferromagnetic (AFM) matrix below the AFM transition temperature T_N, namely magnetic phase separation [12–17]. However, there are still many aspects of interest that are unclear, such as CO transition, the relationship between magnetic properties and structure, and the role of size disorder etc [12].

The interplay between spin, charge, orbital and lattice degrees of freedom in perovskite manganites gives rise to the complex magnetic phase diagram together with transport properties [6, 16–19]. These properties can be tuned by changing the nature and the concentration of trivalent rare-earth or divalent alkaline-earth cations, which determine both the distortions of crystal structure and the concentration of e_g electrons at Mn sites [17]. For instance, the double exchange (DE) interactions between Mn^{3+} and Mn^{4+} can induce ferromagnetism, whereas long-range Coulomb repulsion and Jahn–Teller distortions can result in the localization of Mn^{3+} and Mn^{4+} charges [17, 20]. Carrier concentration, the average size of the cations at the A-site $\langle r_A \rangle$ (defined as $\langle r_A \rangle = \Sigma y_i r_i$, in which r_i is the ionic size and y_i is the fractional occupancy of the ith atoms of A-site) and size mismatching of the A-site dominate the physical properties

[3] Author to whom any correspondence should be addressed.

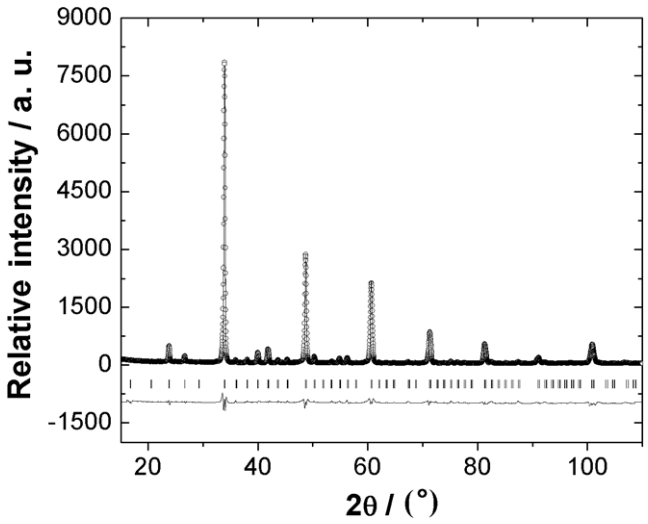

Figure 1. XRD patterns and Rietveld refinement results for $La_{0.1}Ca_{0.9}MnO_3$ at room temperature. The experimental data are shown as dots; the global fitting profile and the difference curve are shown as solid lines; the calculated reflection positions are indicated by stick marks.

of ABO_3-type perovskite manganites [5, 19]. It has been reported that the carrier concentration (or the average valence state of Mn) plays a significant role in transport and CMR properties in electron-doped manganites, whereas size and mismatching effects have less influence [19, 21]. However, the structural factors, including Mn–O bond length, Mn–O–Mn bond angle, $\langle r_A \rangle$ and size mismatching, are also important for the physical properties. For example, a decrease of $\langle r_A \rangle$ in the manganites will induce a tilt of MnO_6 octahedron, favoring the ordering of the Mn^{3+}/Mn^{4+} cations; and crystal structural distortions, or chemical pressure, have a significant effect on the magnetic ordering transition temperature [14, 22–25]. In other words, not only carrier concentration but also structural factors can bring on the complex properties in electron-doped manganites.

In the present paper we investigated the transport and magnetic properties of $CaMnO_3$ doped by La^{3+}, Y^{3+} and Ce^{4+} to determine the effects of carrier concentration and structural factors on the physical properties, as a result of the three ions having different radii and valences. We found that the carrier concentration factor alone cannot describe all the properties including magnetic structure, CO and CMR in electron-doped $CaMnO_3$; the structural factors are also responsible for the physical behavior.

2. Experiment

Polycrystalline specimens of $La_xCa_{1-x}MnO_3$, $Y_xCa_{1-x}MnO_3$ ($x = 0.06$–0.18) and $Ce_xCa_{1-x}MnO_3$ ($x = 0.04$–0.1) were synthesized by a solid state reaction method. Reagent grade $CaCO_3$, MnO_2, La_2O_3, CeO_2 and Y_2O_3 powders in stoichiometric ratio were mixed and calcined at 1273 K for 12 h to achieve decarbonation. Then the mixture was reground, pressed into disk-shaped pellets and sintered at 1573 K for 24 h. Next, the products were reground thoroughly, pressed into pellets again, and then sintered at 1623 K for 36 h. Finally the pellets were slowly cooled down to room temperature in the furnace. All the calcination processes are in air.

X-ray diffraction (XRD) data for all the samples were collected using a Bede D[1] XRD diffractometer with Ni filtered Cu Kα ($\lambda = 0.154\,06$ nm) radiation and scanning (0.02° steps in 2θ) over the range $15° \leqslant 2\theta \leqslant 110°$. Iodometric titration (with the assumption that the valences of Ca, La, Y, Ce and O are +2, +3, +3, +4 and −2, respectively, in acidic solution) was employed to determine the average valence of Mn and excess oxygen content. The results show that the oxygen stoichiometry for all the samples is equal to 3.00 ± 0.01. The oxygen stoichiometry was also checked by thermogravimetric analysis (TGA), using a TA Instruments SDT 2960. The temperature dependences of resistivity were measured using a standard four-probe method. Resistivity, magnetization and Hall measurements were all carried out using a Quantum Design commercial physical properties measurement system (PPMS-9T).

3. Results and discussion

The XRD pattern for $La_{0.1}Ca_{0.9}MnO_3$ at room temperature is shown in figure 1. Other samples have similar XRD patterns. All the sample are single phase with no detectable secondary phase and have an orthorhombic–perovskite structure with the *Pnma* space group. The structural parameters were determined by the Reiveld refinement method, using the profile analysis program Fullprof. According to Shannon's table [26], the ionic radius of Ca^{2+} is smaller than that of La^{3+} but larger than Y^{3+} and Ce^{4+}, so with an increase of x, $\langle r_A \rangle$ increases in the La^{3+} doped series but decreases in Y^{3+} and Ce^{4+} doped series, as shown in figure 2. The size mismatching of the A-site, described by σ^2 ($=\Sigma y_i r_i^2 - \langle r_A \rangle^2$, where r_i is the ionic size and y_i is the fractional occupancy of the ith atoms of the A-site), also varies with x and R ions. σ^2 is relatively minor in La^{3+} doped series and changes little with x, but σ^2 becomes notable and increases with x in Y^{3+} and Ce^{4+} doped series. Ce^{4+} doped samples exhibit the maximum σ^2 and the smallest $\langle r_A \rangle$. The average Mn–O–Mn bond angle $\theta_{Mn-O-Mn}$ for all the samples is significantly decreased from 180°, indicating the strong structural distortions. With an increase of x, $\theta_{Mn-O-Mn}$ increases in the La^{3+} doped series but decreases in Y^{3+} and Ce^{4+} doped series. These results suggest that structural distortion enhances gradually in Y^{3+} and Ce^{4+} doped samples with increase in the doping level. Considering the relatively small ionic radii of Y^{3+} and Ce^{4+}, the substitution of Y^{3+} or Ce^{4+} for Ca^{2+} provides chemical pressure which can induce a constriction of the unit cell and lattice distortions; $\theta_{Mn-O-Mn}$ decreases with doping in the Y^{3+} and Ce^{4+} doped series.

Figure 3 shows the temperature dependence of resistivity ρ for $R_xCa_{1-x}MnO_3$ samples. Compared with undoped semiconducting-like $CaMnO_3$ [5], doping at the Ca site with rare-earth ions first significantly lowers resistivity; then ρ increases with x once the doping content exceeds a certain level (corresponding to an electron concentration of 0.1–0.12 in these series). At a lower temperature, especially, ρ is enhanced

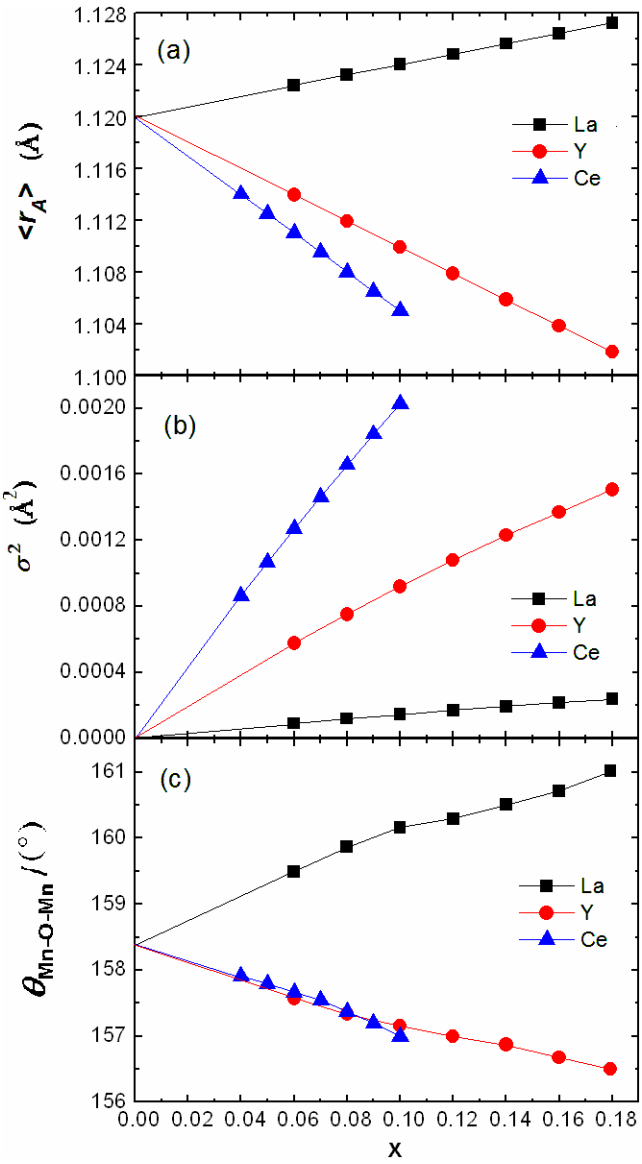

Figure 2. (a) The average cation radius of A-sites $\langle r_A \rangle$, (b) the size mismatching of the A-site σ^2 and (c) the average Mn–O–Mn bond angle $\theta_{Mn-O-Mn}$ versus x for the samples.

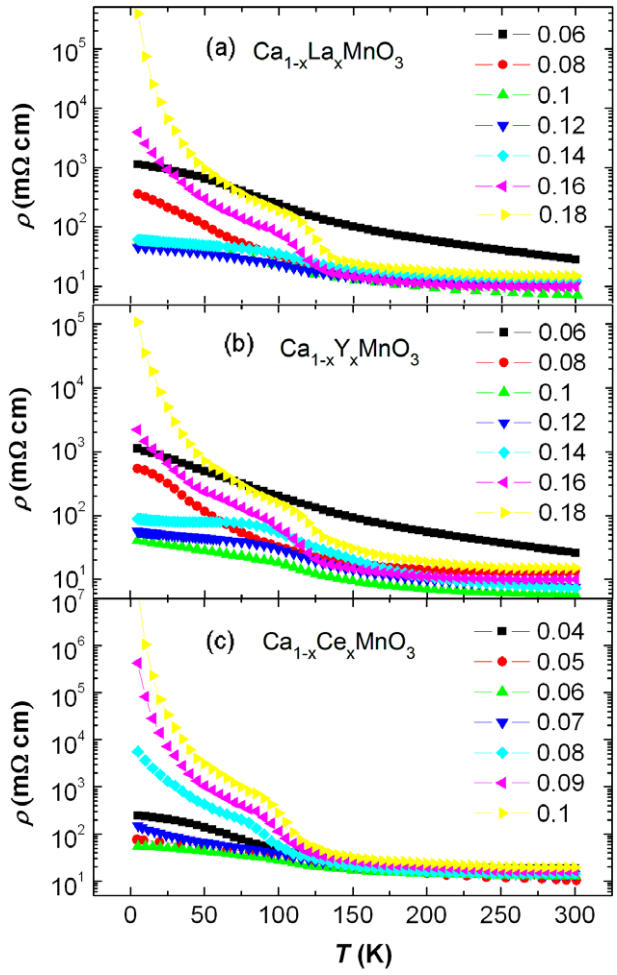

Figure 3. Temperature dependence of resistivity ρ for (a) the $La_xCa_{1-x}MnO_3$ series, (b) the $Y_xCa_{1-x}MnO_3$ series and (c) the $Ce_xCa_{1-x}MnO_3$ series.

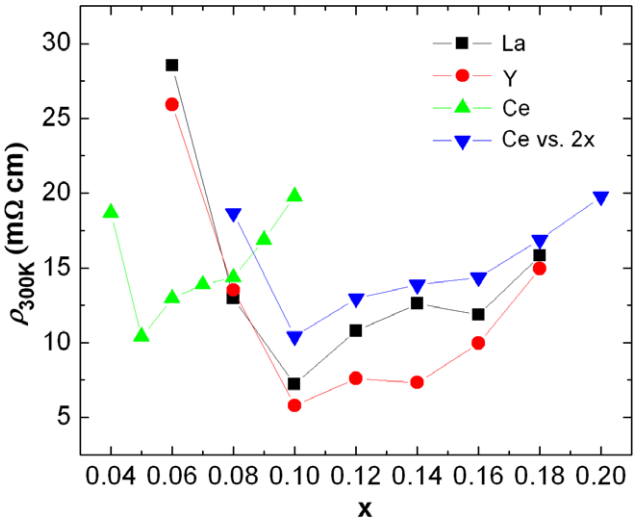

Figure 4. Room-temperature resistivity ρ_{300K} versus x for the samples; the values of ρ versus $2x$ plots for Ce^{4+} doped series are also presented.

dramatically by several orders of magnitude. $La_{0.1}Ca_{0.9}MnO_3$, $Y_{0.1}Ca_{0.9}MnO_3$ and $Ce_{0.05}Ca_{0.95}MnO_3$, respectively, exhibit the lowest room-temperature resistivity $\rho_{300\,K}$ (see figure 4). Although the general trends of ρ–T curves are similar, we should emphasize that the absolute values of ρ for comparable doping levels and the electron concentration dependences in this study are a little different from some previous reports [12, 19, 27]. For instance, there is a minimum in resistivity at low temperature for $La_xCa_{1-x}MnO_3$ at $x = 0.1$–0.12 in this study, but near $x = 0.08$ in [12]; for the $Ce_xCa_{1-x}MnO_3$ system, the smallest resistivity at room temperature occurs at $x = 0.05$ in our results, consistent with Zeng *et al*'s report [27], but different from Maignan *et al*'s result [19], in which it occurs near $x = 0.07$. These differences may be caused by different specimen synthesis processes, since for ceramic samples, resistivity is strongly dependent on grain size, boundary, density, porosity and oxygen content, etc, that can be quite different for samples synthesized by different methods.

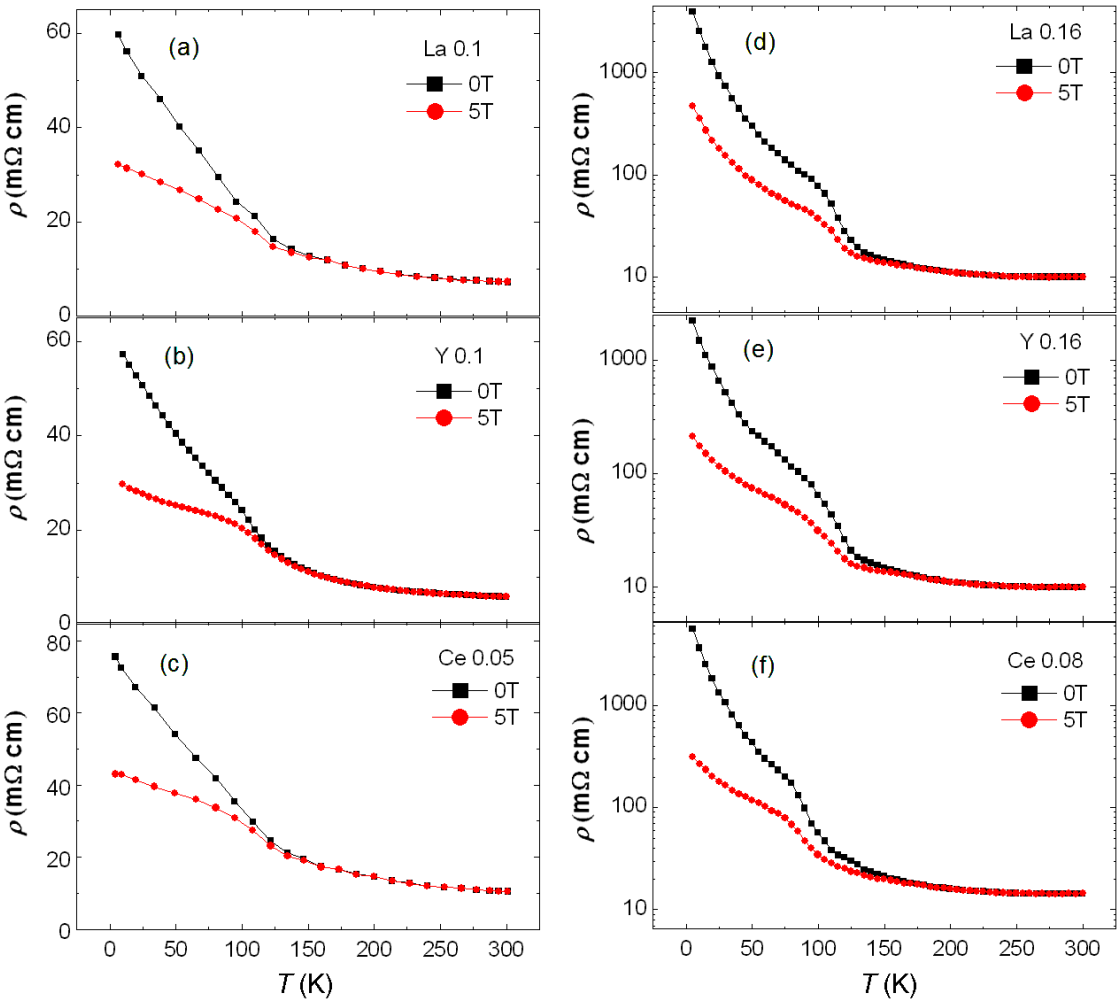

Figure 5. (a)–(f) Temperature dependence of resistivity for the samples under magnetic fields of 0 and 5 T.

The initial reduction of ρ with doping should be attributed to the change in the valence state of Mn by the substitution of R ions considering the electron transport mechanism in perovskite manganites [28, 29]. Based on the valence equilibrium, the substitution of La^{3+}, Y^{3+} or Ce^{4+} for Ca^{2+} will add Mn^{3+} sites and create a large number of electron carriers, which can decrease ρ as a result. Therefore, with the increase of x, the gradual decrease of ρ in this system can be anticipated. However, when x exceeds a certain content, the value of ρ begins to increase, which indicates that other factors must be considered. It has been reported that in an electron-doped $CaMnO_3$ system, when the electron concentration reaches a certain value, charge ordering or local charge ordering can occur below room temperature [5, 12, 21, 30]. The formation of CO with higher x values here has been confirmed by the measurements of magnetic properties as discussed below. Although the CO phenomenon in electron-doped $CaMnO_3$ has been reported by several groups, such as Raveau *et al* and Sudheendra *et al* [5, 12], the origin of CO is still controversial. Nevertheless, energy band calculation suggests that a CO state may be induced in manganites by Jahn–Teller coupling and Coulomb interaction [31, 32]. Since the CO state is a localized electronic state, ρ of a system will be enhanced when CO takes place. Slight electron doping can introduce electrons into the e_g orbital of Mn ions, giving rise to electronic delocalization and the consequent reduction of ρ, but when the doping level increases beyond a certain electron concentration (corresponding to $x \sim 0.1$ for the La^{3+} and Y^{3+} doped series and $x \sim 0.05$ for the Ce^{4+} doped series), CO or local CO behavior takes place, resulting in the localization of electrons and then ρ increases again.

Figure 4 shows the room-temperature resistivity ρ_{300K} for all the samples. Both the values and the evolution of resistivity versus $2x$ plots for Ce^{4+} doped samples are consistent with La^{3+} and Y^{3+} doped samples. Hall measurements show that the carrier concentration of the Ce $2x$ doped sample is comparable to those of the La or Y x doped samples, confirming that the valence of cerium is +4, which is consistent with the x-ray absorption spectroscopy (XAS) results obtained by Zeng *et al* [27]. Considering the tetravalent character of Ce^{4+}, it has to be explained that doping with Ce^{4+} introduces twice as many electrons per substituting atom as doping with La^{3+} or Y^{3+}, and all the electrons introduced by Ce^{4+} doping contribute electrical conductance. This result indicates that electron concentration plays a key role in resistivity behavior.

Such a dependence on electron concentration is also reflected in magnetoresistance properties. Figure 5 presents

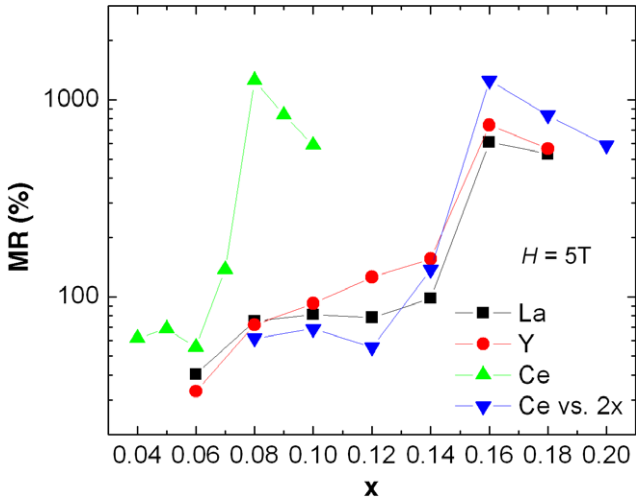

Figure 6. MR versus x for the samples under a 5 T field at 10 K; the values of MR versus $2x$ plots for Ce^{4+} doped series are also presented.

the temperature dependence of resistivity under 0 and 5 T magnetic fields; figure 6 shows the magnetoresistance effect of the samples, in which we define magnetoresistance MR $= \Delta\rho/\rho_H \times 100\% = (\rho_0 - \rho_H)/\rho_H \times 100\%$, where ρ_0 and ρ_H mean ρ at zero field and 5 T field, respectively. At lower temperatures (strictly speaking, below the magnetic ordering transition temperature as discussed below), a large MR is observed. Interestingly, although the samples with an electron concentration of 0.1 have the lowest ρ, their MR are not large; there exists another x value for which magnetoresistance effect is maximum, corresponding to $x \sim 0.16$ for the La^{3+} and Y^{3+} doped series and $x \sim 0.08$ for the Ce^{4+} doped series. Only in this quite narrow range of electron concentration (namely over the range in which the relative electron concentration is 0.16–0.2), can remarkable CMR effects be observed in these electron-doped manganites. This result is similar to previous reports [2, 3, 5, 13]. In fact, the resistance of the samples with an electron concentration of 0.1 is quite low, so that the application of a magnetic field cannot induce a large change in ρ and thus an observable magnetoresistance effect. From figure 6, it can be found that the electron concentration dependence of MR is the same for La^{3+} and Y^{3+} doped series, and it is also consistent with the MR versus $2x$ plot for Ce^{4+} doped series. This MR behavior confirms the crucial influence of electron concentration on electrical transport properties.

From the above comparison, it can be concluded that the electron concentration is the dominant factor in the electrical transport behavior in the electron-doped $CaMnO_3$ system, since the electron concentration dependence of electrical transport properties is nearly identical throughout the three series. When the electron concentration is fixed, all the series have similar electrical transport properties. However, we must emphasize that structural factors (including crystal structural distortions, size disorder, etc) cannot be neglected, because although electron concentration dominates the transport properties, structural factors may play a modulating role in determining the magnitude of a physical

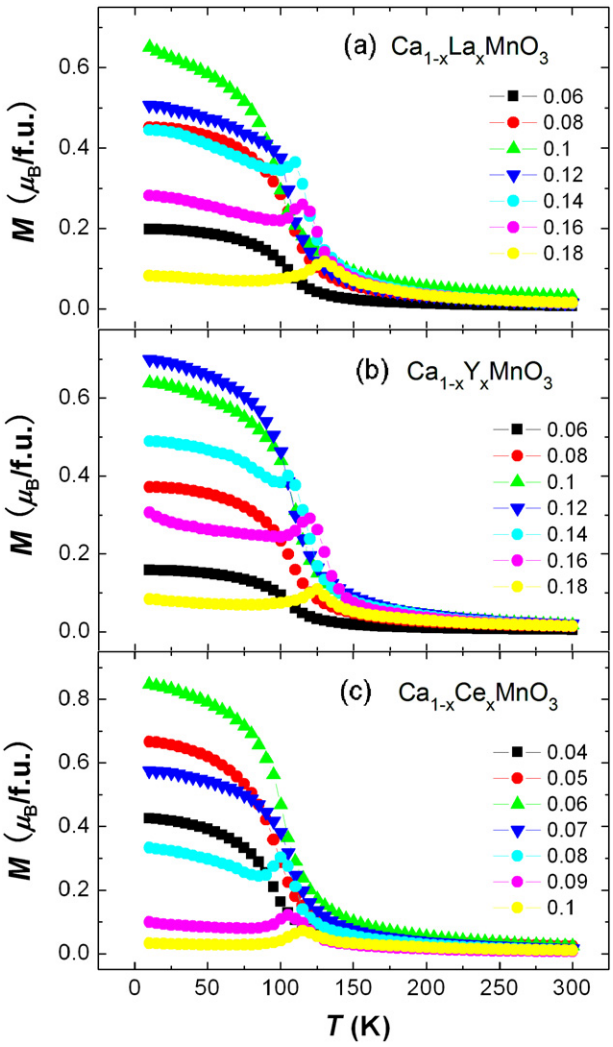

Figure 7. Temperature dependence of dc magnetization M for (a) the $La_xCa_{1-x}MnO_3$ series, (b) the $Y_xCa_{1-x}MnO_3$ series and (c) the $Ce_xCa_{1-x}MnO_3$ series in the field-cooled (FC) mode under a 2 T field.

quantity. For instance, besides electron concentration, ρ is also modulated by the effective e_g bandwidth determined by structural parameters [33]. Since the conduction is governed by the e_g electron, the variation of the effective e_g bandwidth must change the resistivity of the system. That is why $R_xCa_{1-x}MnO_3$ series still exhibit different ρ values even when they have same electron concentration.

Next, we focus on the magnetic properties of this system. The dc magnetization (M) versus temperature curves in the field-cooled (FC) mode with $H = 2$ T are shown in figure 7. We define the magnetic transition temperature (i.e. the spin ordering temperature) T_N as the temperature of the negative maximum slope in the M–T curves, since partial FM behavior is exhibited [5, 19, 27]. Several characters can be found in the M–T curves. (1) With the increase of x, the values of M increase first and then decrease. The maximum of M occurs at $x = 0.1$, 0.12 and 0.06 for R = La, Y and Ce, respectively. (2) For lower doping levels, all the samples exhibit a marked enhancement in M below T_N. (3) For higher x values, a drop of M at low temperature together

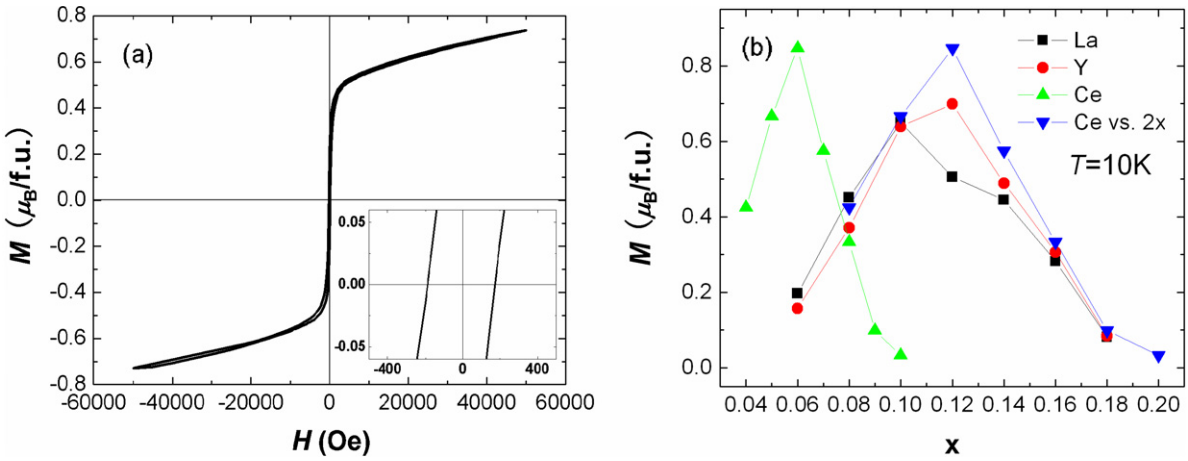

Figure 8. (a) M–H curve for $Y_{0.1}Ca_{0.9}MnO_3$ at 10 K; the inset shows a detail for the region between ±400 Oe. (b) The magnetization at 10 K versus x for the samples (under 2 T field); the values of magnetization versus $2x$ plots for the Ce^{4+} doped series are also presented.

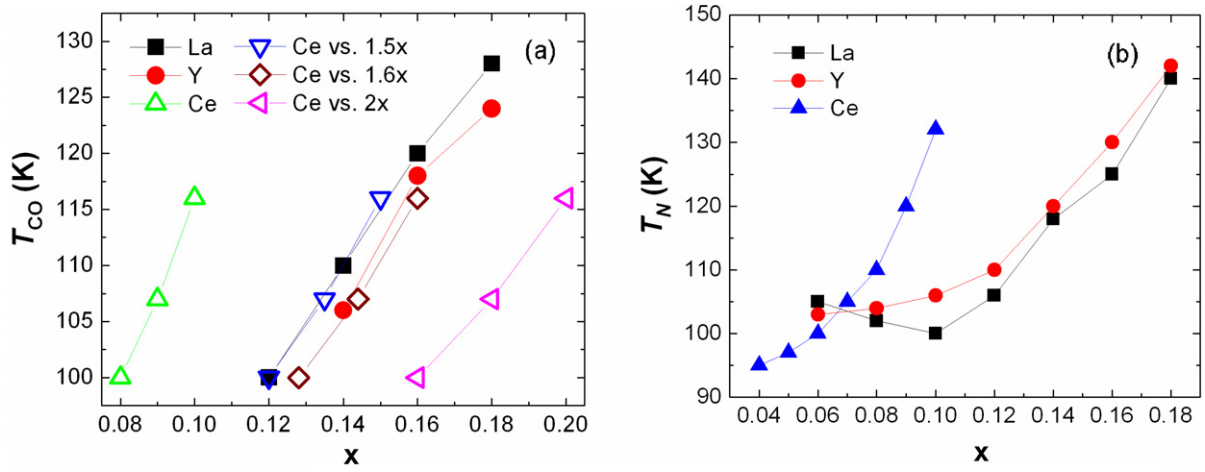

Figure 9. (a) Charge ordering temperature T_{CO} and (b) spin ordering temperature T_N versus x for the samples; T_{CO} versus $1.5x$, $1.6x$ and $2x$ is plotted for Ce^{4+} doped series.

with a peak in the middle temperature are presented in M–T curves. Similar M–T curves were observed in some previous investigations [5, 12, 34]. The M–H curve for $Y_{0.1}Ca_{0.9}MnO_3$ at 10 K is presented in figure 8(a), from which one can see that M increases rapidly with H at lower field, but quite slowly and shows a nearly linear field dependence at higher fields. The value of magnetization under 2 T (∼0.6 μ_B/Mn) is only a little larger than that under 0.4 T (∼0.52 μ_B/Mn). Other samples exhibit similar results. Therefore, although the measurements in [12] were made under 0.4 T, their measured magnetization is not very different from our present study. Although M increases at low temperature, the system is not fully ferromagnetic and shows only small values of saturation magnetization at 10 K. First-principles calculations indicate that it is not possible to induce long-range ferromagnetism in the electron-doped $CaMnO_3$ by any means, which may be because the Fermi level lies on a band edge in these manganites [35].

Previous investigations have pointed out that in electron-doped $CaMnO_3$, the enhancement of M below T_N results from phase separation due to the presence of FM clusters in the AFM matrix [14–17]. The peak in the M–T curve should be attributed to competition between ferromagnetism and antiferromagnetism induced by CO behavior [12, 14–17]. As the temperature decreases, the spin interaction under a magnetic field tends to an enhancement of magnetization (ferromagnetism); but when the temperature decreases through CO (T_{CO}), antiferromagnetism is favored at the expense of ferromagnetism, namely FM interaction cannot develop, so magnetization starts to decrease. Accordingly, a peak in M–T curves appears. The temperature of the appearance of the peak in M–T curves coincides with the temperature at which the largest slope in the ρ–T curves appears, indicating that these two phenomena both arise from the formation of CO. We define the CO temperature T_{CO} as the peak temperature in the M–T curves (shown in figure 9). In fact, the introduction of e_g electrons by lower doping delocalizes the electron state and favors ferromagnetism (appearing in the form of FM clusters), which induces a decrease of resistivity as well as an enhancement of magnetization at low temperature. However,

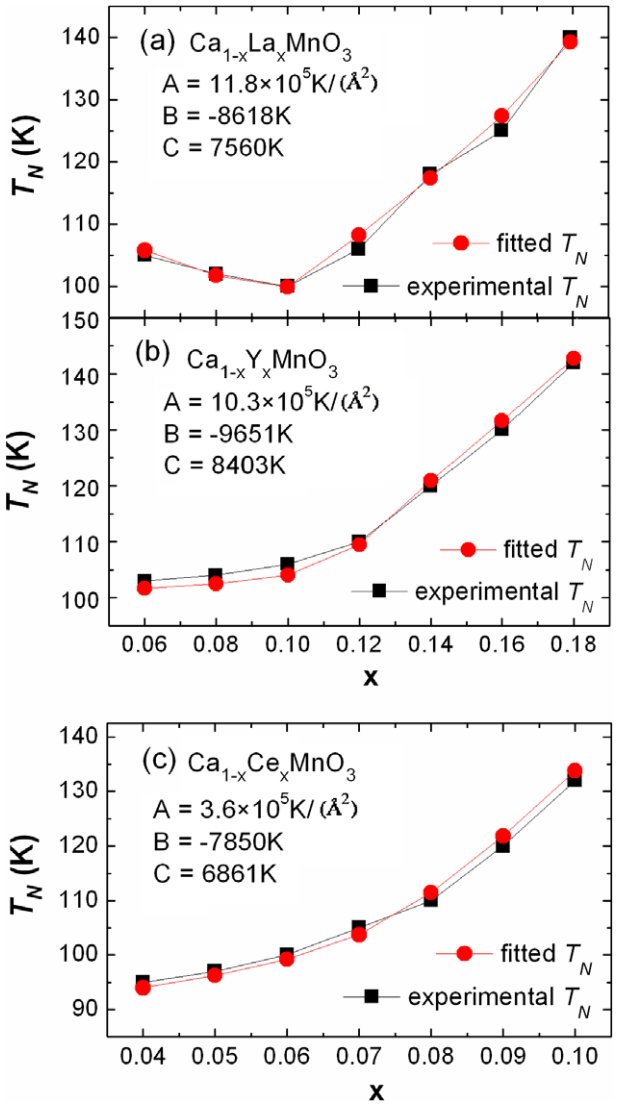

Figure 10. The experimental T_N and fitted T_N with formula (1) as a function of x for the samples; the fitting parameters are also shown.

the appearance of a CO state in samples with a higher electron concentration leads to the localization of electrons, which not only gives rise to the observable increase in ρ below T_{CO}, but also favors antiferromagnetism. As a result, ferromagnetism cannot fully develop, whereas the competition between ferromagnetism and antiferromagnetism brings on quite small saturation magnetization and a peak in the M–T curves. Finally, with the increase in x, the localized electron state predominates and antiferromagnetism develops rapidly in the system, so that the intensity of M and peaks in M–T curves decrease gradually and the system becomes a homogeneous AFM phase.

From figure 8, one can see the variation of M at 10 K versus x clearly. La^{3+} doped series exhibits the largest magnetization with an electron concentration of 0.1 but Y^{3+} and Ce^{4+} doped series have the largest magnetization with an electron concentration of 0.12. The dependence of magnetization on electron concentration is not completely the same, which is in contrast to the resistivity and MR behavior. This result suggests that the electron concentration factor alone cannot describe the magnetic properties of the system fully, namely the effect of enhancement by structural factors.

Figure 9 presents the variation of T_{CO} and T_N with x for three series. Because ferromagnetism and antiferromagnetism coexist in the system, it is reasonable to define its magnetic ordering temperature T_N in the same way as the definition of FM ordering temperature T_C and adopt the peak temperature as CO temperature T_{CO} [5, 19, 22, 27]. For all three series T_{CO} rises as x increases. The CO state forms fully when the electron concentration exceeds 0.12, 0.14 and 0.16 in La^{3+}, Y^{3+} and Ce^{4+} doped series, respectively. In addition, when the three series show nearly equal T_{CO}, they have neither the same doping level nor the same electron concentration. Moreover, when the three series have the same electron concentration, T_{CO} of the La^{3+} doped sample is slightly higher than that of the Y^{3+} doped sample, but much higher than for the Ce^{4+} doped sample. Both T_{CO} versus x and $2x$ plots for Ce^{4+} doped samples are inconsistent with La^{3+} and Y^{3+} doped series; however, if T_{CO} versus $1.5x$ or $1.6x$ are plotted for Ce^{4+} doped samples, one can see that they agree with La^{3+} and Y^{3+} doped series very well. These results distinctly demonstrate that the magnetic properties and CO behavior of the electron-doped $CaMnO_3$ system are determined by the coupling of electron concentration and structural factors. The carrier concentration factor alone cannot describe all these properties. Maybe a new function, consisting of carrier concentration and structural parameters, could describe the magnetic and CO behavior satisfactorily.

It can been seen in figure 9 that as x increases, the spin ordering temperature T_N in La^{3+} doped series decreases first from 105 down to 100 K (corresponding to $x = 0.1$) and then rises up to 140 K, but T_N in Y^{3+} and Ce^{4+} doped series increases monotonically from 103 K to 142 K and 95 K to 132 K, respectively. From the variation and the values of T_N, it seems that there is no direct relationship between T_N and electron concentration. In contrast, a crystal structural distortion has a significant effect on the magnetic transition temperature in manganite perovskites. Recent research shows that T_N of perovskite Mn oxides is determined by the crystal structural parameters and can be well described as a function of $\theta_{Mn-O-Mn}$ and σ^2 [14, 22]. Based on Chmaissem *et al*'s model [22], we fit T_N of the three series with

$$T_N = A\sigma^2 + B\langle\cos^2\theta\rangle + C. \quad (1)$$

As shown in figure 10, the values of T_N fitted using formula (1) are in good agreement with the observed values of T_N for all the samples, which clearly indicates that the crystal structural factors (σ^2 and $\theta_{Mn-O-Mn}$), rather than the carrier concentration factor, have a crucial effect on T_N of electron-doped perovskite manganite systems. These results also demonstrate that crystal structure and magnetic properties are strongly coupled to each other in this family.

4. Conclusions

Investigations of the transport and magnetic properties of La^{3+}, Y^{3+} and Ce^{4+} doped $CaMnO_3$ series reveal that

in electron-doped $CaMnO_3$ system the electrical transport properties are mostly dependent on carrier concentration, but the magnetic properties and CO behavior are strongly coupled to crystal structure, since the change in carrier concentration alone cannot explain the variation of magnetization and CO temperature T_{CO} with x. As for the spin ordering temperature T_N, it seems that T_N is determined by crystal structural parameters alone, which reveals that crystal structure and magnetic properties are strongly coupled to each other. From the transport properties to magnetic properties, the influence of structural factors on the system is gradually enhanced.

Acknowledgments

This work is supported by the National Natural Science Foundation of China (grant nos 50672019 and 10804024).

References

[1] Uehara M, Mori S, Chen C H and Cheong S W 1999 *Nature* **399** 560
[2] Martin C, Maignan A, Hervieu M and Raveau B 1999 *Phys. Rev.* B **60** 12191
[3] Chmaissem O, Dabrowski B, Kolesnik S, Mais J, Jorgensen J D and Short S 2003 *Phys. Rev.* B **67** 094431
[4] Pissas M and Kallias G 2003 *Phys. Rev.* B **68** 134414
[5] Raveau B, Maignan A, Martin C and Hervieu M 1998 *Chem. Mater.* **10** 2641
[6] Liu G L, Zhou J S and Goodenough J B 2001 *Phys. Rev.* B **64** 144414
[7] Millis A J, Littlewood P B and Shraiman B I 1995 *Phys. Rev. Lett.* **74** 5144
[8] Jin S, O'Bryan H M, Tiefel T H, McCormack M and Rhodes W W 1995 *Appl. Phys. Lett.* **66** 382
[9] Tomioka Y, Kuwahara H, Asamitsu A, Kasai M and Tokura Y 1997 *Appl. Phys. Lett.* **70** 3609
[10] Moreo A, Yonuki S and Dagotto E 1999 *Science* **283** 2034
[11] Tokura Y and Nagaosa N 2000 *Science* **288** 462
[12] Sudheendra L, Raju A R and Rao C N R 2003 *J. Phys.: Condens. Matter* **15** 895
[13] Neumeier J J and Goodwin D H 1999 *J. Appl. Phys.* **85** 5591
[14] Hirano S, Sugiyama J, Noritake T and Tani T 2004 *Phys. Rev.* B **70** 094419
[15] Mahendiran R, Maignan A, Martin C, Hervieu M and Raveau B 2000 *Phys. Rev.* B **62** 11644
[16] Martin C, Maignan A, Hervieu M, Raveau B, Jirák Z, Savosta M M, Kurbakov A, Trounov V, André G and Bourée F 2000 *Phys. Rev.* B **62** 6442
[17] Respaud M, Broto J M, Rakoto H, Vanacken J, Wagner P, Martin C, Maignan A and Raveau B 2001 *Phys. Rev.* B **63** 144426
[18] Hejtmánek J, Jirák Z, Maryško M, Martin C, Maignan A, Hervieu M and Raveau B 1999 *Phys. Rev.* B **60** 14057
[19] Maignan A, Martin C, Damay F and Raveau B 1998 *Chem. Mater.* **10** 950
[20] Zener C 1951 *Phys. Rev.* **82** 403
[21] Jorge M M E, Nunes M R, Maria R S and Sousa D 2005 *Chem. Mater.* **17** 2069
[22] Chmaissem O, Dabrowski B, Kolesnik S, Mais J, Brown D E, Kruk R, Prior P, Pyles B and Jorgensen J D 2001 *Phys. Rev.* B **64** 134412
[23] Garcia-Munoz J L, Fontcuberta J, Suaaidi M and Obradors X 1996 *J. Phys.: Condens. Matter* **8** L787
[24] Rodriguez-Martinez L M and Attfield J P 1996 *Phys. Rev.* B **54** R15622
[25] Attfield J P, Kharlanov A L and McAllister J A 1998 *Nature* **394** 157
[26] Shannon R D 1976 *Acta Crystallogr.* A **32** 751
[27] Zeng Z, Greenblatt M and Croft M 2001 *Phys. Rev.* B **63** 224410
[28] Jakob G, Westerburg W, Martain F and Adrian H 1998 *Phys. Rev.* B **58** 14966
[29] Chun S H, Salamon M B, Lyanda-Geller Y, Goldbart P M and Han P D 2000 *Phys. Rev. Lett.* **84** 757
[30] Caspi E N, Avdeev M, Short S, Jorgensen J D, Lobanov M V, Zeng Z, Greenblatt M, Thiyagarajan P, Botez C E and Stephens P W 2004 *Phys. Rev.* B **69** 104402
[31] Yunoki S, Hotta T and Dagotto E 1999 *Phys. Rev. Lett.* **84** 3714
[32] Popovic Z and Satpathy S 2002 *Phys. Rev. Lett.* **88** 197201
[33] Medarde M, Mesot J, Lacorre P, Rosenkranz S, Fischer P and Gobrecht K 1995 *Phys. Rev.* B **52** 9248
[34] Chiba H, Kikuchi M, Kusaba K, Muraoka Y and Syono Y 1996 *Solid State Commun.* **99** 499
[35] Vijaya Sarathy K, Vanitha P V, Seshadri R, Cheetham A K and Rao C N R 2001 *Chem. Mater.* **13** 787